ADVANCED FUNCTIONAL MATERIALS
www.afm-journal.de

Layer-by-Layer Controlled Perovskite Nanocomposite Thin Films for Piezoelectric Nanogenerators

Younghoon Kim, Keun Young Lee, Sun Kak Hwang, Cheolmin Park, Sang-Woo Kim, and Jinhan Cho**

Perovskite nanoparticle-based nanocomposite thin films strictly tailored using unconventional layer-by-layer (LbL) assembly in organic media for piezoelectric nanogenerators (NGs) are demonstrated. By employing sub-20-nm $BaTiO_3$ nanoparticles stabilized by oleic acid ligands (i.e., OA-BTO_{NPs}) and carboxylic acid (COOH)-functionalized polymers, such as poly(acrylic acid) (PAA), the resulting OA-BTO_{NP}/PAA nanocomposite multilayers are prepared by exploiting the high affinity between the COOH groups of PAA and the BTO_{NPs}. The ferroelectric and piezoelectric performance of the (PAA/OA-BTO_{NP})$_n$ thin films can be precisely controlled by altering the bilayer number, inserted polymer type, and OA-BTO_{NP} size. It is found that the LbL assembly in nonpolar solvent media can effectively increase the quantity of adsorbed OA-BTO_{NPs}, resulting in the dramatic enhancement of electric power output from the piezoelectric NGs. Furthermore, very low leakage currents are detected from the (PAA/OA-BTO_{NP})$_n$ thin films for obtaining highly reliable power-generating performance of piezoelectric NGs.

1. Introduction

Perovskite-type ferroelectric oxide (PFO) materials possess the properties of spontaneous polarization and high dielectric constants, in addition to exhibiting piezoelectric and pyroelectric behaviors. As a result, PFO materials have attracted considerable attention because they can be directly applied to energy-harvesting devices to scavenge and convert various types of energy (i.e., mechanical and thermal energy, etc.) into electrical energy,[1–18] as well as to other technical applications, such as batteries, sensors, magnetoelectric devices.[19–21] Recently, the successful preparation of piezoelectric nanogenerators (NGs), which can harvest mechanical energy from our surrounding living environments, was demonstrated using piezoelectric PFO materials such as $BaTiO_3$ (BTO),[2–5] $ZnSnO_3$,[6–8] (K, Na) NbO_3,[9,10] PMN-PT,[11,12] and Pb(Zr,Ti) O_3 (PZT).[13–17] The results offer significant potential for various technological applications, such as remote/wireless data transmission, battery charging, and the powering of electronic devices.

BTO has been regarded as one of the most technologically promising PFO materials for use in piezoelectric NGs because of its strong piezoelectric properties and the environmental advantages that it offers over lead-based PFO ceramics such as PZT. However, little experimental consensus exists on the critical size at which the size-dependent ferroelectricity of the BTO nanoparticles (BTO_{NPs}) is suppressed, whereby the critical size of the BTO_{NPs} is generally recognized to be approximately 10–20 nm.[22] Most studies of BTO-based devices have focused on the use of large BTO_{NPs} (>100 nm),[4] BTO nanotubes (approximately 5 μm in length or longer)[23] or vacuum-deposited BTO layers with high-temperature annealing.[3] Further, although a nanocomposite thin film has been regarded as a very attractive structure for large-scale flexible piezoelectric NGs due to its facile size scalability, cost-effectiveness, and mechanical robustness,[8] a high degree of control over the film/layer dimensions and a uniform internal structure without the requirement of binders or additives to prevent NP segregation or agglomeration are still very challenging for the realization of high-performance nanocomposite thin film-based piezoelectric NGs.

With respect to the fabrication of nanocomposite films, the layer-by-layer (LbL) assembly method has demonstrated the highest potential and versatility for the preparation of nanocomposite films with tailored thicknesses, compositions, and functionalities achieved through complementary interactions.[24–34] LbL assemblies can also be effectively applied to various substrates, irrespective of their size or shape. However, the traditional LbL assembly of electrostatically charged inorganic NPs in aqueous solvents relies on electrostatic properties of NP surface, hence the direct application of this approach for

Y. Kim, Prof. J. Cho
Department of Chemical and Biological Engineering
Korea University
Seoul 136-713, Republic of Korea
E-mail: jinhan71@korea.ac.kr
K. Y. Lee, Prof. S.-W. Kim
School of Advanced Materials Science and Engineering
Sungkyunkwan University (SKKU)
Suwon 440-746, Republic of Korea
E-mail: kimsw1@skku.edu
S. L. Hwang, Prof. C. Park
Department of Materials Science and Engineering
Yonsei University
Seoul 120-749, Republic of Korea
Prof. S.-W. Kim
SKKU Advanced Institute of Nanotechnology (SAINT)
Center for Human Interface Nanotechnology (HINT)
Sungkyunkwan University (SKKU)
Suwon 440-746, Republic of Korea

DOI: 10.1002/adfm.201401599

nanocomposite thin film-based high-performance piezoelectric NGs is undesirable because of low quantities of charged NPs and large leakage currents.

Here, we give the first report of perovskite BTO_{NPs}-based nanocomposite thin films strictly tailored using unconventional LbL assembly in organic media for high-performance piezoelectric NGs. The nanocomposite multilayers are composed of monodisperse oleic acid (OA)-stabilized PFO-type NPs (i.e., OA-BTO_{NPs}) with sub-20-nm sizes and poly(acrylic acid) (PAA) with carboxylic acid (COOH) moieties and can be prepared using LbL assembly in organic media. It should also be noted that carrying out the LbL assembly in nonpolar solvent media can increase the quantity of adsorbed OA-BTO_{NPs} because no electrostatic repulsion occurs among the OA-BTO_{NPs}. The adsorbed quantity of BTO_{NPs} within the nanocomposites significantly affects the piezoelectric power generating performance of the resulting NGs. The formation of the $(PAA/OA\text{-}BTO_{NP})_n$ multilayers is very effective to secure highly reliable operation of NGs with large power output and low leakage currents.

2. Results and Discussion

OA-BTO_{NPs} with sizes of approximately 13 nm (13-nm OA-BTO_{NPs}) were synthesized using a hydrothermal process and then were dispersed in a nonpolar solvent, either toluene or hexane (see Experimental section). High-resolution transmission electron microscopy (HR-TEM) imaging showed that the 13-nm OA-BTO_{NPs} were well defined and highly monodisperse, exhibiting cube-like shapes and a narrow size distribution as shown in **Figure 1**a. The image inset in Figure 1a indicates that the as-synthesized 13-nm OA-BTO_{NPs} were highly crystalline with a lattice distance of 2.86 Å in the <110> crystalline direction.[35] To investigate more precisely the crystalline structure of the 13-nm OA-BTO_{NPs}, we performed X-ray diffraction (XRD) analysis. The XRD peaks of the 13-nm OA-BTO_{NPs} coincided with those of the previously reported pseudocubic BTO structure (Figure 1b).[35,36] Specifically, it should be noted that no $BaCO_3$ peaks, which indicate the presence of a secondary phase, were present in our XRD patterns. These results indicate that highly monodisperse 13-nm OA-BTO_{NPs} with cube-like shapes and highly crystalline structures can be easily prepared under atmospheric conditions without the formation of a byproduct (i.e., $BaCO_3$).[37]

Raman spectroscopy was used to investigate the tetragonality of 13-nm OA-BTO_{NPs}, where this structure is directly related to the ferroelectric properties of this material. Generally, at temperatures higher than the Curie temperature ($T_c \approx 130$ °C), BTO exhibits paraelectric properties characteristic of a cubic structure (space group *Pm3m*) with 12 Raman-inactive optical modes ($3F_{1u}+1F_{2u}$).[38] However, at temperatures below T_c, BTO transforms from a Raman-inactive cubic structure to a Raman-active tetragonal structure (space group *P4mm*) as a result of a reduction in crystal symmetry. Tetragonal BTO exhibits ferroelectric properties as a result of the lattice distortion of the Ti^{4+} ion coordinated with the octahedral oxygen groups.[38,39] We observed Raman peaks from the 13-nm OA-BTO_{NPs} at 184, 261, 304, 520, and 716 cm^{-1}, which correspond to the Raman-active transverse (TO) and longitudinal (LO) modes of A_1(LO), A_1(TO), B_1+E(TO+LO), E(TO)+A_1(TO), and A_1(LO)+E(LO), respectively (Figure 1c). The two strong Raman peaks at 304 and 520 cm^{-1} imply the presence of an asymmetric Ti^{4+} ion in the BTO unit cell. It was reported that these two peaks are gradually disappeared with decreasing BTO_{NP} size and with increasing temperature.[38]

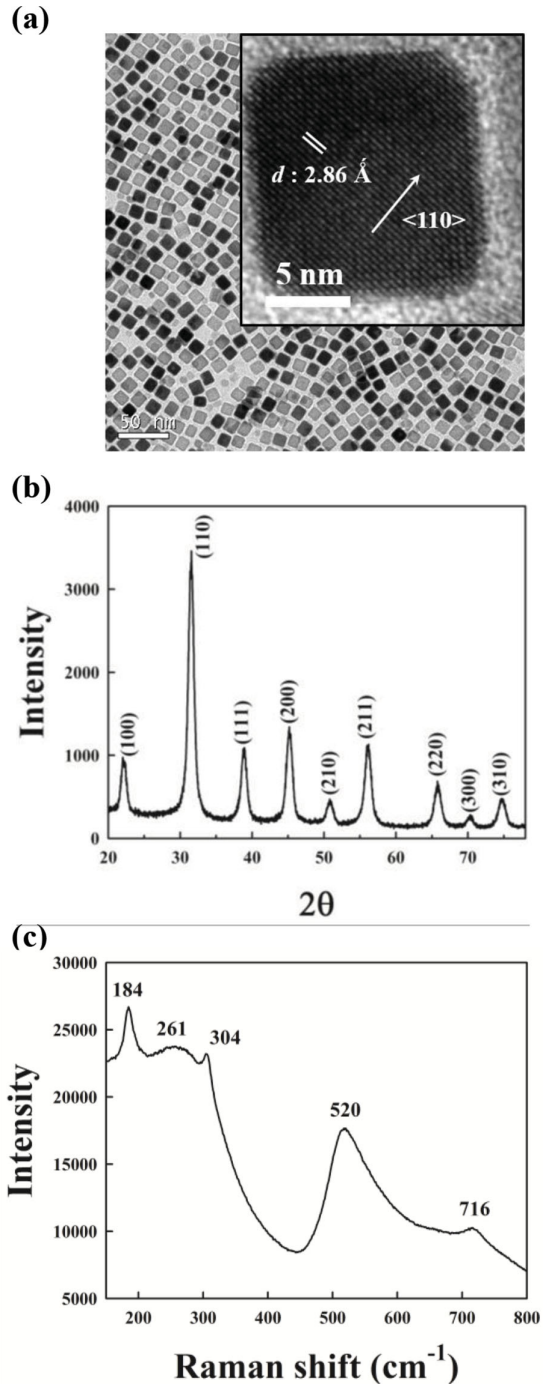

Figure 1. a) HR-TEM image, b) XRD pattern, and c) Raman spectrum of 13-nm OA-BTO_{NPs}.

Based on these results, multilayers composed of OA-BTO_{NPs} dispersed in a nonpolar solvent and PAA in ethanol were

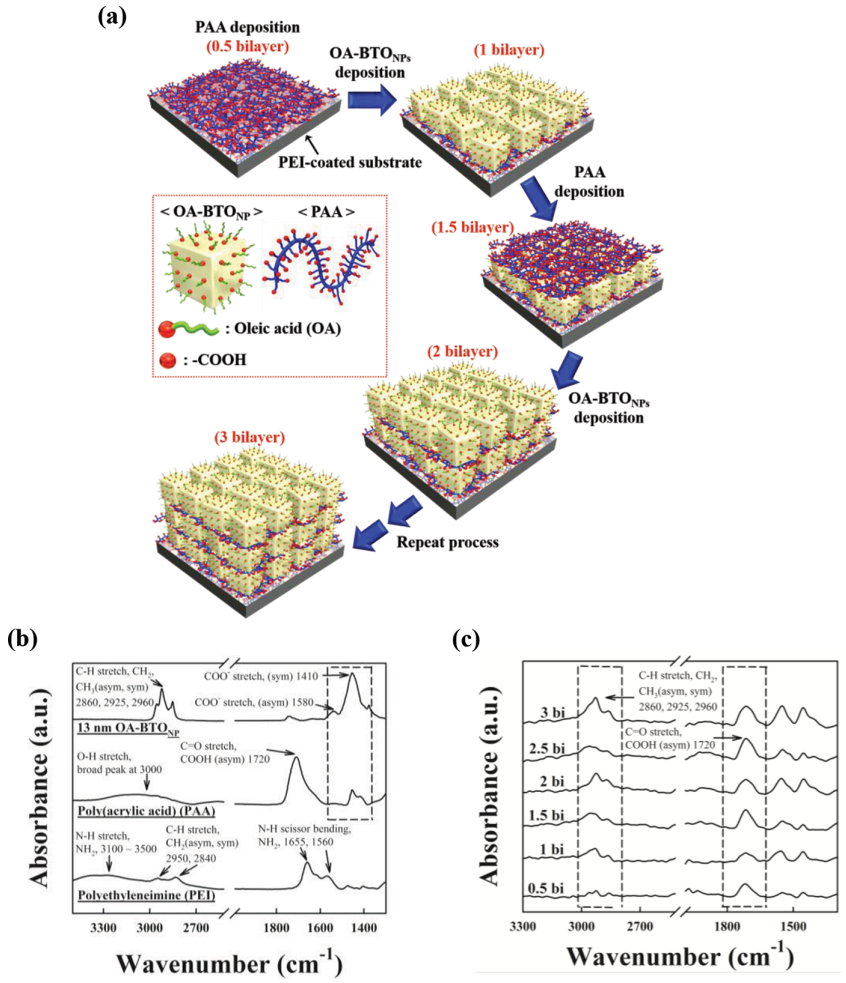

Figure 2. a) A schematic illustration of the LbL growth of a PAA/13- or 8-nm OA-BTO$_{NP}$ multilayer. b) FT-IR spectra of 13-nm OA-BTO$_{NP}$, PAA, and PEI, respectively. c) FT-IR spectra of the (PAA/13-nm OA-BTO$_{NP}$)$_n$ multilayers as a function of the number of bilayers.

prepared via LbL assembly (**Figure 2**a). The adsorption mechanism for the LbL multilayer was characterized using Fourier-transform infrared spectroscopy (FT-IR). Although the pristine OA ligands have the carboxylic acid (–COOH) moieties, these groups are bound to the surface of metal oxide such as BTO$_{NPs}$ as a form of carboxylate ion (–COO$^-$) groups.[40] Therefore, the observed C–H stretching (2860, 2925, and 2960 cm^{-1}) and COO$^-$ stretching (1580 and 1410 cm^{-1}) peaks originate from the long aliphatic chains and the COO$^-$ groups of the OA ligands bound to the BTO$_{NPs}$, respectively. The OA ligands were primarily adsorbed onto the crystal faces with high Ba ion densities because all six coordinate positions of the Ti ion are occupied by hydroxyl groups in the OA-BTO$_{NPs}$ system (see Experimental section).[35] The FT-IR spectrum of the PAA exhibited both strong absorption peaks for the COOH stretching vibration mode (1720 cm^{-1}) and a relatively weak absorption peak for the COO$^-$ stretching mode (1580 cm^{-1} and 1410 cm^{-1}) (Figure 2b). Therefore, the –COO$^-$ stretching modes at 1580 and 1410 cm^{-1}, which arise from the OA ligands, nearly overlap with the peaks from the PAA.

We investigated the absorption peak traces from the OA ligands at 2860, 2925, and 2960 cm^{-1} (i.e., the C–H stretching of the long aliphatic chains) and from the PAA at 1720 (i.e., the COOH stretching vibration mode), 1580 and 1410 cm^{-1} (i.e., the COO$^-$ stretching mode) by alternately the deposition of PAA and OA-BTO$_{NPs}$ onto the substrates (Figure 2c). The absorption peaks originating from the PAA and OA ligands gradually intensified as the bilayer number (n) increased from 0.5 to 3. Such phenomena imply that the PAA layer is deposited onto the OA-BTO$_{NPs}$ using additional covalent bonds between the COO$^-$ group of the PAA and the Ti^{4+} ions within the TiO_6 octahedra of the OA-BTO$_{NPs}$ without OA ligand exchange. In this case, the COO$^-$ group of PAA bound to the surface of BTO$_{NPs}$ originated from the COOH as well as the COO$^-$ group of pristine PAA chains.

The LbL growth of the PAA/13-nm OA-BTO$_{NP}$ multilayers was quantitatively monitored using quartz crystal microgravimetry (QCM) measurements (**Figure 3**a). The mass changes (Δm) were calculated from the frequency changes (ΔF) of the PAA and 13-nm OA-BTO$_{NP}$ layers adsorbed onto the crystal surfaces. Alternating the deposition of the PAA (2 mg mL^{-1}) and 13-nm OA-BTO$_{NPs}$ (10 mg mL^{-1}) resulted in $-\Delta F$ values of 65 ± 4 (Δm approximately equal to 1205 ng cm^{-2}) and 150 ± 6 Hz (Δm approximately equal to 2638 ng cm^{-2}) per layer, respectively. Based on these results, the calculated number density of the 13-nm OA-BTO$_{NPs}$ in each layer was approximately 1.99×10^{11} cm^{-2} using a BTO density of 6.02 g cm^{-3} and the cubic volume of the 13-nm OA-BTO$_{NP}$. In addition, we confirmed that the adsorbed amount of 13-nm OA-BTO$_{NPs}$ onto the PAA-coated QCM electrode could also be controlled as a function of the concentration of BTO$_{NP}$ solution (see Figure S1 in the Supporting Information). Therefore, the adsorbed amount of 13-nm OA-BTO$_{NPs}$ onto PAA layer was further increased up to approximately 4275 ng cm^{-2} ($-\Delta F \approx 242$ Hz) when the concentration of OA-BTO$_{NP}$ solution was increased up to 30 mg mL^{-1}. Additionally, we investigated the film thickness of the multilayers as a function of the bilayer number using cross-sectional field-emission scanning electron microscopy (FE-SEM). The cross-sectional FE-SEM images indicate that the total film thickness of the (PAA/13-nm OA-BTO$_{NP}$)$_n$ multilayers increased linearly from 74 to 223 nm as the number of bilayers was increased from 5 to 20 (Figure 3b). Through qualitative investigation using UV–Vis spectroscopy, we also confirmed that in addition to OA-BTO$_{NPs}$, a variety of hydrophobic transition metal oxide NPs (i.e., OA-TiO_2, OA-Fe_3O_4, and OA-MnO_x) could be LbL-assembled with COOH-polymers (i.e., PAA) (see Figure S2 in the Supporting Information).

Based on these results, the polarization-electric field (*P*–*E*) curves of the (PAA/13-nm OA-BTO$_{NP}$)$_{n\ =\ 20,\ 40,\ \text{and}\ 60}$ multilayers under an electric field of ±500 kV cm^{-1} and a frequency

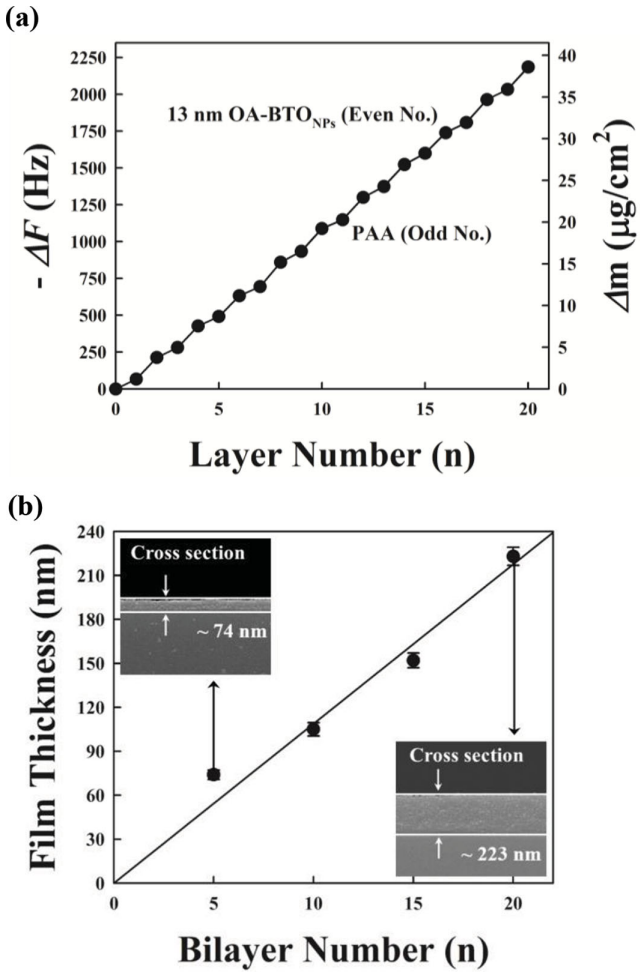

Figure 3. a) The frequency changes ($\triangle F$) and mass changes ($\triangle m$) in the adsorbed PAA and 13-nm OA-BTO$_{NPs}$ with increasing periodic layer number, investigated using QCM measurement. b) The film thickness of the (PAA/13-nm OA-BTO$_{NP}$)$_n$ multilayers as a function of the number of bilayers. The inset shows cross-sectional FE-SEM images of the multilayers.

of 1 kHz were used to investigate the ferroelectric properties of the material (**Figure 4**a). The multilayers were sandwiched between platinum (Pt) bottom and gold (Au) top electrodes, measuring approximately 400 μm × 400 μm in size. The measured remnant polarization (P_r) and coercive electric field (E_c) values for the multilayers were approximately 4.43 μC cm^{-2} and 168.9 kV cm^{-1}, respectively, for n = 20, 6.05 μC cm^{-2} and 146.7 kV cm^{-1} for n = 40, and 8.06 μC cm^{-2} and 141.9 kV cm^{-1} for n = 60. As the bilayer number increased, the ferroelectric performance of the multilayers improved, P_r increased, and E_c decreased. Although numerous research groups have proposed various mechanisms regarding the effect of ferroelectric film thickness,[41–44] a possible mechanism for our system can be explained using the film/electrode interfacial blocking layer model.

The proposed model suggests that when ferroelectric materials are sandwiched between the bottom and top electrodes, an intermediate (or dead) layer forms at the film/electrode interface, which results in poor or non-ferroelectric properties due to the interface stress and/or the chemical damage caused by the thermal evaporation of the top electrode.[43] These ferroelectric phenomena were also observed in the multilayers based on 8-nm OA-BTO$_{NPs}$, which are closer to the critical size for ferroelectricity (see Figure S3 in the Supporting Information). However, the P_r of the 8-nm OA-BTO$_{NP}$ films decreased slightly compared to that of the 13-nm OA-BTO$_{NP}$ films because of the effect of the grain size on the ferroelectricity.

Figure 4b shows the dielectric constant (ε) and dielectric loss (tan δ) for the (PAA/13-nm OA-BTO$_{NP}$)$_{n = 20, 40, and 60}$ multilayers measured at frequencies ranging from 10^2 to 10^6 Hz. The ε of the multilayers increased slightly from 12.0 to 12.4 at a frequency of 1 kHz as the bilayer number was increased from 20 to 60. Although the ε for the approximately 220-nm-thick multilayers (i.e., 20 bilayers) was significantly smaller than that of bulk BTO (ε was approximately 1500 at 1 kHz) due to the insertion of a non-ferroelectric polymer and the formation of numerous non-ferroelectric boundaries among the neighboring OA-BTO$_{NPs}$,[45] nanocomposite films with a relatively high ε of approximately 12 were obtained primarily from films with a thickness on the order of 20 μm filled with micrometer-sized ceramic particles.[46] It is reasonable to conclude that the good ferroelectric and dielectric properties demonstrated in the (PAA/13-nm OA-BTO$_{NP}$)$_n$ multilayers are also related to extremely low levels of leakage current within the films.

To confirm this relationship, we measured the current-electric field of the multilayers under DC voltages (Figure 4c). The leakage currents for all samples were less than ~10^{-6} A over the electric field range of ± 500 kV cm^{-2}. The observed phenomena indicate that despite being produced at room temperature, the LbL-assembled (PAA/13-nm OA-BTO$_{NP}$)$_n$ multilayers can exhibit better insulating properties than conventional polycrystalline BTO (>100 nm) and thermally annealed BTO thin films.[44,47] However, the (poly(ethylene imine) (PEI)/13-nm OA-BTO$_{NP}$)$_n$ multilayers generated significant leakage currents due to the hydrophilicity of PEI, despite the application of an identical electric field (see Figure S4 in the Supporting Information).

Based on the abovementioned results, we fabricated BTO$_{NPs}$-based nanocomposite thin film-based piezoelectric NGs using a device structure of indium tin oxide (ITO)-coated plastic substrate/(PAA/OA-BTO$_{NP}$)$_n$ multilayers with an aluminum (Al) top electrode as shown in **Figure 5**a. A periodic pushing force was applied to the top of the multilayered piezoelectric NG with an effective area of 1 cm^2 in the direction perpendicular to the top electrode. Figure 5b shows the output voltage and current generated from the LbL-assembled (PAA/13-nm OA-BTO$_{NP}$)$_n$ multilayers. As the bilayer number (n) was increased from 20 to 100, the output voltage and current increased to approximately 1.8 V and 700 nA, respectively, under a compressive force (5.2 kgf) and without an electrical poling process. Reportedly, the unpoled dipoles within the ferroelectric film can be aligned by the application of an external stress instead of an electric field. Therefore, ferro- and piezoelectricity can be generated and improved due to the external force-induced poling effect.[48,49] These results indicate that the piezoelectric performance of our materials can be easily improved by increasing the quantity of OA-BTO$_{NPs}$.

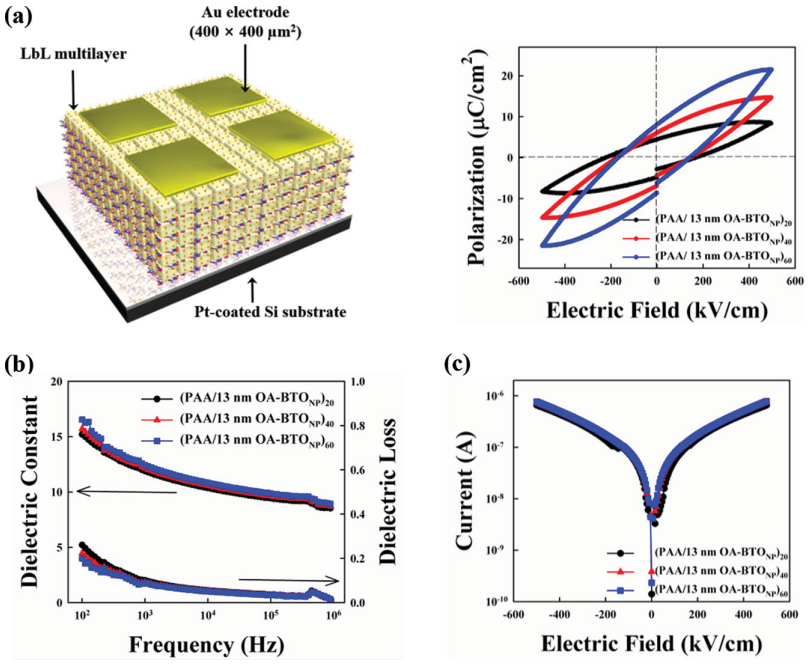

Figure 4. a) A schematic illustration and polarization-electric field (*P*–*E*) curve of (PAA/13-nm OA-BTO$_{NP}$)$_n$ (n = 20, 40, and 60) multilayers under an electric field of ± 500 kV cm^{-1}. b) Frequency-dependent dielectric behavior and c) leakage current curves (under an electric field of ± 500 kV cm^{-1}) for (PAA/13-nm OA-BTO$_{NP}$)$_n$ (n = 20, 40, and 60) multilayers.

Additionally, the polarity-switching tests indicate that the output voltage and current of the piezoelectric NGs originated from the PAA/13-nm OA-BTO$_{NP}$ multilayers and not the measurement system (**Figure 6**a and Figure S5 in the Supporting Information). When the voltage and current meters were initially connected to the piezoelectric NG, the positive pulses were predominantly recorded during pushing. When the voltage and current meters were connected with reverse polarity, the pulses were also reversed. However, the magnitudes of the output voltages and currents under both conditions were nearly identical. To examine further the electrical and mechanical stability of the multilayered piezoelectric NGs, we performed cycling tests to determine the piezoelectric stability of the associated output voltages and currents. Stable voltage and current peaks were maintained during approximately 4500 cycles at 1.5 Hz (3000 s) (Figure 6b).

We further investigated the influence of compressive forces on the piezoelectric performance by measuring the output voltage and current of a device containing 100 bilayers as a function of the applied compressive force (**Figure 7**a). As the compressive force was increased from 0.8 to 5.2 kgf, the output voltage and current increased from approximately 0.4 V and 60 nA to 1.8 V and 700 nA, respectively. These results demonstrate that a degree of external compressive force can significantly affect the aligned electric dipoles and the resultant piezoelectric performance of (PAA/OA-BTO$_{NP}$)$_n$ multilayers without an additional poling process. Similar piezoelectric properties were also observed in the (PAA/8-nm OA-BTO$_{NP}$)$_n$ multilayers, although their output performance was slightly lower than that of the 13-nm OA-BTO$_{NPs}$-based films for the same number of bilayers and applied compressive force. The piezoelectric NG composed of (PAA/8-nm OA-BTO$_{NP}$)$_{100}$ multilayers exhibited an output voltage and current of approximately 1.6 V and 650 nA, respectively, under a compressive force of 5.2 kgf (see Figure S6 in the Supporting Information). However, the output voltage and current of the piezoelectric NG composed of (PEI/13-nm BTO$_{NP}$)$_{100}$ multilayer was much smaller than that of (PAA/13-nm BTO$_{NP}$)$_{100}$ multilayer due to the high leakage current generated within PEI/13-nm BTO$_{NP}$ multilayer (see Figure S7 in the Supporting Information). These results clearly show that the piezoelectric performance of

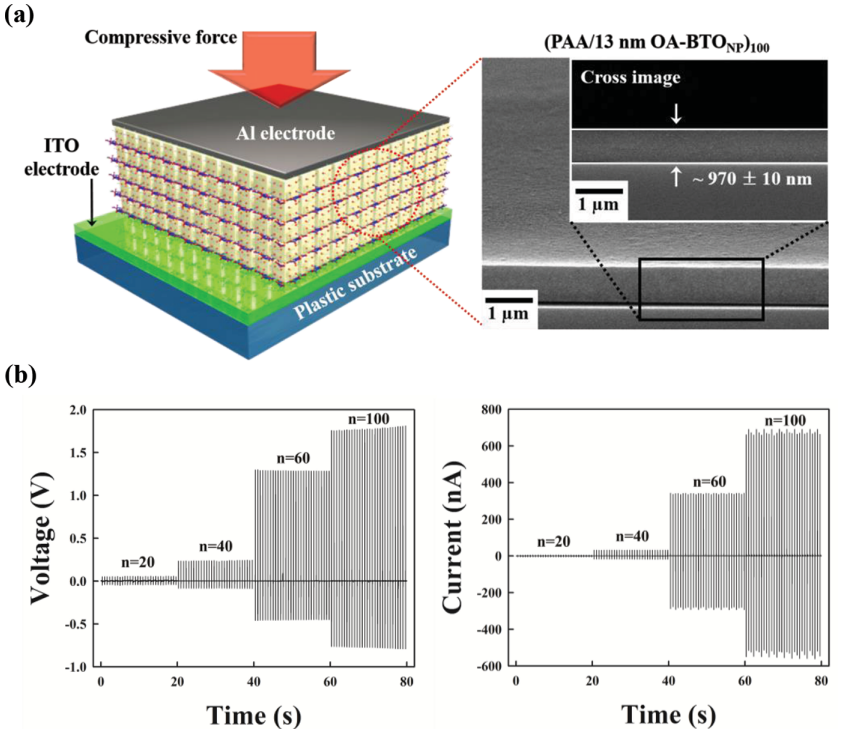

Figure 5. a) A schematic illustration of a piezoelectric NG based on a (PAA/13- or 8-nm OA-BTO$_{NP}$)$_n$ multilayer. b) The output voltage and current of the multilayered piezoelectric NGs as a function of the number of bilayers (n).

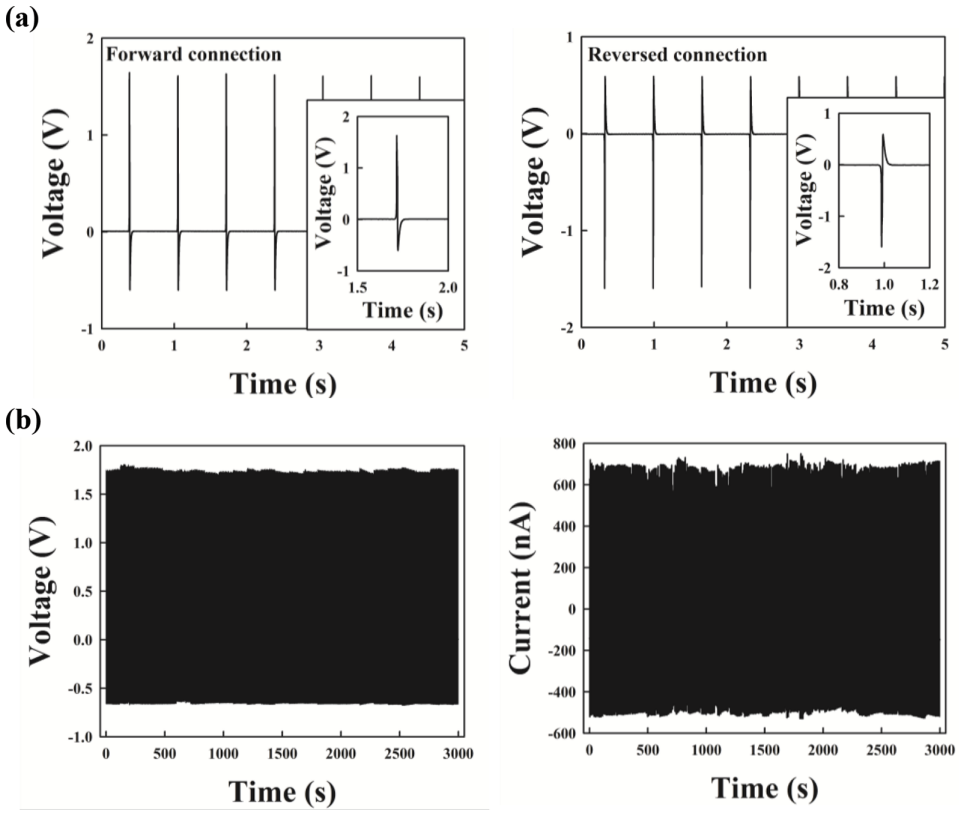

Figure 6. a) The polarity-switching tests of the (PAA/13-nm OA-BTO_{NP})$_{100}$ multilayered piezoelectric NG. b) The electrical stability test of the (PAA/13-nm OA-BTO_{NP})$_{100}$ multilayered piezoelectric NG using a periodic pushing machine.

OA-BTO_{NP}-based multilayers strongly depends on the type of the inserted polymers.

3. Conclusions

We demonstrated that PFO NP-based nanocomposite multilayers can be successfully prepared using LbL assembly and that the ferroelectric and piezoelectric properties of these materials can be improved by altering the number of bilayers, NP size, and type of inserted polymer, despite the extremely small domain size of the BTO_{NPs} with respect to ferroelectric behaviors. The LbL assembly in nonpolar solvent media effectively increased the quantity of adsorbed OA-BTO_{NPs}, resulting in the dramatic enhancement of electric power output from the piezoelectric NGs. Furthermore, very low leakage currents were detected from the (PAA/OA-BTO_{NP})$_n$ thin films. The resulting LbL-assembled PAA/13-nm OA-BTO_{NP} nanocomposite thin film-based NG produced the output voltage and current of about 1.8 V and 700 nA, respectively.

4. Experimental Section

Synthesis of OA-BTO_{NPs}: The synthetic procedure of approximately 13-nm-sized OA-BTO_{NPs} was modified from that of 20-nm-sized BTO_{NPs} proposed by Dang et al.[35] First, titanium bis(ammonium lactate) dihydroxide (TALH) (1.2 mmol, 0.3534 g) was added to the aqueous solution (24 mL) containing barium hydroxide octahydrate (1.2 mmol, 0.3786 g). Then, 5 M NaOH solution (5 mL), oleic acid (OA) (8.4 mmol, 2.3726 g), tert-butylamime (19.2 mmol, 1.4043 g) were sequentially added to the reaction mixture under magnetic stirring.The mixture was subsequently transferred to 30 mL teflon-lined stainless steel autoclave. The sealed autoclave was mechanically stirred at 210 °C for 72 h. The resulting solution was centrifuged (8000 rpm, 10 min) three times with excess ethanol to remove the surfactant residuals. The precipitated white product was then dispersed in toluene or hexane (40 mL). After then, centrifugation process (1000 rpm, 2 min) was repeated three times to remove the precipitates. 8 nm-sized OA-BTO_{NPs} were synthesized by changing the molar ratio of tert-butylamine from 19.2 mmol to 14.4 mmol.

Synthesis of OA-stabilized Hydrophobic NPs: A variety of hydrophobic NPs, such as TiO_2,[37] Fe_3O_4,[50] and MnO_x,[51] were synthesized using OA as a stabilizer in a nonpolar solvent, following the methods previously reported by other research groups.

Build-up of LbL-assembled Multilayers: The concentrations of OA-BTO_{NPs} in toluene and PAA in ethanol were adjusted to 10 and 2 mg mL^{-1}, respectively. Quartz and silicon substrates were washed with an RCA solution (H_2O: NH_3: H_2O_2 = 5: 1: 1 v/v/v). A solution of PAA in ethanol was first coated onto the PEI-coated substrate for 10 min, followed by washing twice with ethanol. The OA-BTO_{NPs} in toluene were sequentially deposited onto the PAA-coated substrate for 20 min, followed by washing with toluene. This process was repeated until the desired number of layers was deposited (Note: the abovementioned dip LbL assembly process could be replaced by the spin LbL-assembly method of 15 s at 4000 rpm for the deposition and washing conditions of PAA and OA-BTO_{NP}).[52] The LbL assembly shown in our study is based on the high affinity between the surfaces of the

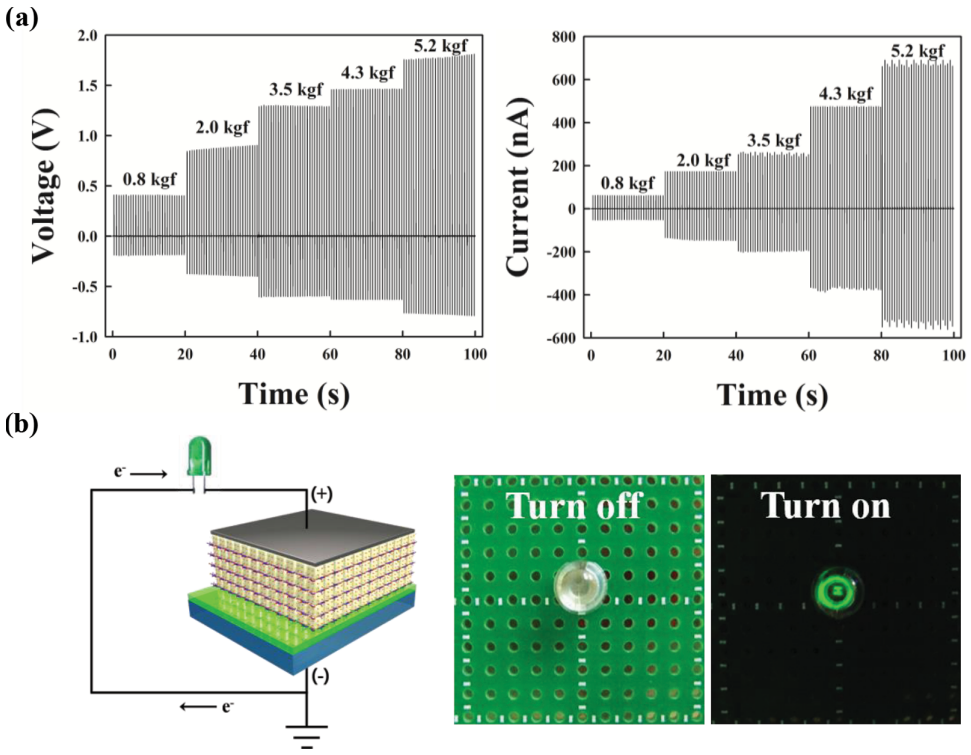

Figure 7. a) Output voltage and current of (PAA/13-nm OA-BTO_{NP})$_{100}$ multilayer-based piezoelectric NGs with different compressive forces. b) A captured image showing a light-emitting diode lit up by the power output generated from the (PAA/13-nm OA-BTO_{NP})$_{100}$ piezoelectric NG.

PFO-type NPs, such as BTO_{NP}, and the carboxylic acid groups of a polymer, such as PAA. After LbL assembly, the OA ligands bound to the Ba ions are not removed because the carboxylic acid groups of the PAA are bonded to the Ti^{4+} ions within the TiO_6 octahedra of the OA-BTO NPs without the ligand exchange of OA.

Measurements: HR-TEM (a JEOL JEM 3000F microscope) was carried out on as-synthesized OA-BTO_{NPs}. The cross-sectional images of (PAA/OA-BTO_{NP})$_n$ multilayer films were characterized by FE-SEM (Hitachi S-4300). Crystal structures of OA-BTO_{NPs} were examined using X-ray diffraction (XRD) at room temperature. Data collection was performed in the 2θ range from 15 to 60° using Cu Kα radiation ($\lambda = 1.54$ Å, Model: Bruker D8 Discover, Germany). Raman spectra at room temperature were measured using a LabRam ARAMISS Raman Spectroscopy (Horiba Jobin-Yvon) using the 633 nm line of a He-Ne laser. Vibrational spectra were measured by FT-IR (iS10 FT-IR, Thermo Fisher) in the absorbance and attenuated total reflection (ATR) modes. The sample chamber was purged with N_2 gas for 2 h to eliminate water and CO_2 prior to conducting the FT-IR measurement. A FT-IR spectrum for the (PAA/OA-BTO_{NP})$_n$ film deposited onto an Au-coated substrate was obtained from 200 scans with an incident angle of 80°. The acquired raw data was plotted after baseline correction, and the spectrum was smoothed using spectrum analyzing software (OMNIC, Nicolet). The UV- vis spectra were measured using a Perkin Elmer Lamda 35 UV–vis spectrometer. A quartz crystal microgravimetry (QCM) device (QCM200, SRS) was used to investigate the mass of material deposited after each adsorption step. The resonance frequency of the QCM electrodes was approximately 5 MHz. The adsorbed mass of OA-BTO_{NP} and PAA, $\triangle m$, was calculated from the change in QCM frequency, $\triangle F$, using the Sauerbrey equation:[53]

$$\Delta F(\mathrm{Hz}) = -\frac{2F_0^2}{A\sqrt{\rho_q \mu_q}}\Delta m$$

Here, F_0 (approximately 5 MHz) is the fundamental resonance frequency of the crystal, A is the electrode area, and ρ_q (approximately 2.65 g cm^{-2}) and μ_q (approximately 2.95×10^{11} g cm^{-2} s^{-2}) are the shear modulus and density of quartz, respectively. This equation can be simplified as follows:

$$\Delta F(\mathrm{Hz}) = -56.6 \times \Delta m_A$$

where $\triangle m_A$ is the mass change per quartz crystal unit area in μg cm^{-2}. The PAA/OA-BTO_{NP} multilayers adsorbed onto the QCM electrode can be considered rigid, evenly distributed, and sufficiently thin films, thereby satisfying the Sauerbrey equation.[54,55] The ferroelectric polarization–electric field (P–E) curves for all samples were measured using a Precision Materials Analyzer for ferroelectric test systems (RADIANT TECHNOLOGIES, INC., Model: P-LC100). The dielectric constant and dielectric loss were measured using a 4284A Precision LCR Meter (Agilent). The output voltage and current measurements for the piezoelectric performance were performed using a digital phosphor oscilloscope (Tektronix, Model: DPO 3052). Periodic pushing forces for these measurements were applied to PAA/OA-BTO_{NP} multilayers using a vibration test system (Labworks Inc., Model: pa-151).

Fabrication of Nanocomposite Thin Film-based Piezoelectric NGs: The PAA/OA-BTO_{NP} multilayers for the measurement of ferroelectric polarization and dielectric behavior were prepared on Pt-coated (100 nm) silicone substrates. A 400-μm-sized Au (100 nm) film was used as the top electrode. Piezoelectric NGs were fabricated using PAA/OA-BTO_{NP} multilayers fabricated on ITO-coated plastic substrates, and Al was used as the top electrode for the piezoelectric NG.

Supporting Information

Supporting Information is available from the Wiley Online Library or from the author.

Acknowledgements

Y.K. and K.Y.L. contributed equally to this work. This work was supported by NRF grant funded by the Ministry of Science, ICT & Future Planning (MSIP) (2010-0029106; 2009-0083540) and by the Human Resources Development Program of KETEP grant (NO. 20134010200600) funded by the Korea government Ministry of Trade, Industry and Energy. This work was also supported by Samsung Research Funding Center of Samsung Electronics under Project Number SRFC-MA1301-07.

Received: May 18, 2014
Revised: June 23, 2014
Published online: August 18, 2014

[1] Z. L. Wang, W. Wu, *Angew. Chem. Int. Ed.* **2012**, *51*, 11700.
[2] Z. Wang, J. Hu, A. P. Suryavanshi, K. Yum, M.-F. Yu, *Nano Lett.* **2007**, *7*, 2966.
[3] K.-I. Park, S. Xu, Y. Liu, G.-T. Hwang, S.-J. L. Kang, Z. L. Wang, K. J. Lee, *Nano Lett.* **2010**, *10*, 4939.
[4] K.-I. Park, M. Lee, Y. Liu, S. Moon, G.-T. Hwang, G. Zhu, J. E. Kim, S. O. Kim, D. K. Kim, Z. L. Wang, K. J. Lee, *Adv. Mater.* **2012**, *24*, 2999.
[5] S.-H. Shin, Y.-H. Kim, M. H. Lee, J.-Y. Jung, J. Nah, *ACS Nano* **2014**, *8*, 2766.
[6] J. M. Wu, C. Xu, Y. Zhang, Z. L. Wang, *ACS Nano* **2012**, *6*, 4335.
[7] J. M. Wu, K.-H. Chen, Y. Zhangc, Z. L. Wang, *RSC Adv.* **2013**, *3*, 25184.
[8] K. Y. Lee, D. Kim, J.-H. Lee, T. Y. Kim, M. K. Gupta, S.-W. Kim, *Adv. Funct. Mater.* **2014**, *24*, 37.
[9] J. H. Jung, M. Lee, J.-I. Hong, Y. Ding, C.-Y. Chen, L.-J. Chou, Z. L. Wang, *ACS Nano* **2011**, *5*, 10041.
[10] Y. Yang, J. H. Jung, B. K. Yun, F. Zhang, K. C. Pradel, W. Guo, Z. L. Wang, *Adv. Mater.* **2012**, *24*, 5357.
[11] M. B. Starr, J. Shi, X. Wang, *Angew. Chem. Int. Ed.* **2012**, *51*, 5962.
[12] G.-T. Hwang, H. Park, J.-H. Lee, S. Oh, K.-I. Park, M. Byun, H. Park, G. Ahn, C. K. Jeong, K. No, H. Kwon, S.-G. Lee, B. Joung, K. J. Lee, *Adv. Mater.* **2014**, *28*, 4880.
[13] Y. Qi, J. Kim, T. D. Nguyen, B. Lisko, P. K. Purohit, M. C. McAlpine, *Nano Lett.* **2011**, *11*, 1331.
[14] M. Ali, D. Prakash, T. Zillger, P. K. Singh, A. C. Hübler, *Adv. Energy Mater.* **2013**, *4*, 1300427.
[15] S. Xu, B. J. Hansen, Z. L. Wang, *Nat. Commun.* **2010**, *1*, 93.
[16] K.-I. Park, C. K. Jeong, J. Ryu, G.-T. Hwang, K. J. Lee, *Adv. Energy Mater.* **2013**, *3*, 1539.
[17] K.-I. Park, J. H. Son, G.-T. Hwang, C. K. Jeong, J. Ryu, M. Koo, I. Choi, S. H. Lee, M. Byun, Z. L. Wang, K. J. Lee, *Adv. Mater.* **2014**, *26*, 2514.
[18] X. Li, S.-G. Lu, X.-Z. Chen, H. Gu, X.-S. Qian, Q. M. Zhang, *J. Mater. Chem. C* **2013**, *1*. 23.
[19] B. T. Matthias, *Science* **1951**, *113*, 591.
[20] M. J. Dicken, L. A. Sweatlock, D. Pacifici, H. J. Lezec, K. Bhattacharya, H. A. Atwater, *Nano Lett.* **2008**, *8*, 4048.
[21] A. M. Ionescu, *Nat. Nanotechnol.* **2012**, *7*, 83.
[22] M. J. Polking, M.-G. Han, A. Yourdkhani, V. Petkov, C. F. Kisielowski, V. V. Volkov, Y. Zhu, G. Caruntu, A. P. Alivisatos, *Nat. Mater.* **2012**, *11*, 700.
[23] Z.-H. Lin, Y. Yang, J. M. Wu, F. Zhang, Z. L. Wang, *J. Phys. Chem. Lett.* **2012**, *3*, 3599.
[24] G. Decher, *Science* **1997**, *277*, 1232.
[25] F. Caruso, R. A. Caruso, H. Möhwald, *Science* **1998**, *282*, 1111.
[26] J. Schmitt, G. Decher, W. J. Dressick, S. L. Brandow, R. E. Geer, R. Shashidhar, J. M. Calvert, *Adv. Mater.* **1997**, *9*, 61.
[27] M. Yoon, J. Choi, J. Cho, *Chem. Mater.* **2013**, *25*, 1735.
[28] B. Lee, Y. Kim, S. Lee, Y. S. Kim, D. Wang, J. Cho, *Angew. Chem. Int. Ed.* **2010**, *49*, 359.
[29] J. Hong, W. Bae, S. Oh, H. Lee, K. Char, F. Caruso, J. Cho, *Adv. Mater.* **2007**, *19*, 4364.
[30] Y. Ko, H. Baek, Y. Kim, M. Yoon, J. Cho, *ACS Nano* **2013**, *7*, 11445.
[31] Y. Kim, C. Lee, I. Shim, D. Wang, J. Cho, *Adv. Mater.* **2010**, *22*, 5140.
[32] Y. Ko, Y. Kim, H. Baek, J. Cho, *ACS Nano* **2011**, *5*, 9918.
[33] J. D. Berrigan, T.-S. Kang, Y. Cai, J. R. Deneault, M. F. Durstock, K. H. Sandhage, *Adv. Funct. Mater.* **2011**, *21*, 1693.
[34] Y. Kim, K. Kook, S. K. Hwang, C. Park, J. Cho, *ACS Nano* **2014**, *8*, 2419.
[35] F. Dang, K. Mimura, K. Kato, H. Imai, S. Wada, H. Haneda, M. Kuwabara, *Nanoscale* **2012**, *4*, 1344.
[36] S. Adireddy, C. Lin, B. Cao, W. Zhou, G. Caruntu, *Chem. Mater.* **2010**, *22*, 1946.
[37] D. Pan, N. Zhao, Q. Wang, S. Jiang, X. Ji, L. An, *Adv. Mater.* **2005**, *17*, 1991.
[38] M. B. Smith, K. Page, T. Siegrist, P. L. Redmond, E. C. Walter, R. Seshadri, L. E. Brus, M. L. Steigerwald, *J. Am. Chem. Soc.* **2008**, *130*, 6955.
[39] M. DiDomenico, S. H. Wemple, S. P. S. Porto, R. P. Bauman, *Phys. Rev.* **1968**, *174*, 522.
[40] S. Sun, *Adv. Mater.* **2006**, *18*, 393.
[41] S. B. Ren, C. J. Lu, J. S. Liu, H. M. Shen, Y. N. Wang, *Phys. Rev. B* **1996**, *54*, R14337.
[42] S. T. Mckinstry, C. A. Randall, J. P. Maria, C. Theis, D. G. Schlom, J. Shepard Jr., K. Yamakawa, *Mater. Res. Soc. Symp. Proc.* **1996**, *433*, 363.
[43] P. K. Larsen, G. J. M. Dormans, D. J. Taylor, P. J. van Veldhoven, *J. Appl. Phys.* **1994**, *76*, 2405.
[44] L. Huang, Z. Chen, J. D. Wilson, S. Banerjee, R. D. Robinson, I. P. Herman, R. Laibowitz, S. O'Brien, *J. Appl. Phys.* **2006**, *100*, 034316.
[45] P. Kim, N. M. Doss, J. P. Tillotson, P. J. Hotchkiss, M.-J. Pan, S. R. Marder, J. Li, J. P. Calame, J. W. Perry, *ACS Nano* **2009**, *3*, 2581.
[46] R. Schroeder, L. A. Majewski, M. Grell, *Adv. Mater.* **2005**, *17*, 1535.
[47] M. H. Song, Y. H. Lee, T. S. Hahn, M. H. Oh, K. H. Yoon, *J. Appl. Phys.* **1996**, *79*, 3744.
[48] A. Y. Emelyanov, N. A. Pertsev, A. L. Kholkin, *Phys. Rev. B* **2002**, *66*, 214108.
[49] A. Gruverman, B. J. Rodriguez, A. I. Kingon, R. J. Nemanich, A. K. Tagantsev, J. S. Cross, M. Tsukada, *Appl. Phys. Lett.* **2003**, *83*, 728.
[50] S. Sun, H. Zeng, D. B. Robinson, S. Raoux, P. M. Rice, S. X. Wang, G. Li, *J. Am. Chem. Soc.* **2004**, *126*, 273.
[51] H. B. Na, J. H. Lee, K. An, Y. L. Park, M. Park, I. S. Lee, D.-H. Nam, S. T. Kim, S.-H. Kim, S.-W. Kim, K.-H. Lim, K.-S. Kim, S.-O. Kim, T. Hyeon, et al. *Angew. Chem.* **2007**, *119*, 5493.
[52] J. Cho, K. Char, S.-Y. Kim, J.-D. Hong, K.-B. Lee, *Adv. Mater.* **2001**, *13*, 1076.
[53] D. Buttry, *Advances in Electroanalytical Chemistry: Applications of the QCM to Electrochemistry*, Marcel Dekker, New York **1991**.
[54] D. Thid, J. J. Benkoski, S. Svedhem, B. Kasemo, J. Gold, *Langmuir* **2007**, *23*, 5878.
[55] A. G. Hemmersam, K. Rechendorff, F. Besenbacher, B. Kasemo, D. S. Sutherland, *J. Phys. Chem. C* **2008**, *112*, 4180.